An empirical approach to predicting heat transfer within single & twin skin automotive exhaust systems

C. D. Bannister and C. J. Brace
University of Bath

J. Taylor, T. Brooks and N. Fraser
Mahle Powertrain, UK

ABSTRACT

This paper describes the further development of an exhaust system model based on the experimental characterisation of heat transfer in a series of different pipe sections. Building on previous work published in this journal by the authors, this study was undertaken to improve the operating range, accuracy and usability of the original model as well as introducing the ability to model twin skin exhaust sections with an air gap.

Convective heat transfer relationships for nine stainless steel exhaust bend sections of varying wall thicknesses and radiuses were experimentally characterised over a range of steady state conditions. In each case a correlation between observed Reynolds number (Re) and Nusselt number (Nu) was developed. Based on measured experimental data, a generic model was built using Matlab/Simulink capable of predicting the relationship between Nusselt number and Reynolds number for previously unseen pipe geometries falling within the experimental design range. To further develop the usefulness of the model, fifteen twin skin test sections, intended to represent a range of geometries applicable to production automotive gasoline exhaust systems, were also fabricated and characterised. Within the model, both skins of each pipe section were split into five axial and radial elements with the inner and outer skins linked via the modelling of free convection and radiation between them.

The predicted Reynolds-Nusselt relationships for each bend section and twin skin configuration were validated using transient experimental data over a portion of the US06 drive cycle. The final model demonstrated improved accuracy of exhaust gas temperature predictions, compared with previous model iterations, with typical errors of less than $\pm$1% and a mean error over the US06 cycle of +0.2%.

INTRODUCTION

Automotive manufacturers are under increasing pressure balancing the necessity to comply with current and forthcoming emissions legislation, with the need to reduce costs in light of the current global economic conditions. There is always a degree of iteration between the original powertrain and vehicle design, and changes made in response to findings from development programmes and re-packaging in alternative platforms. Prototype manufacture and testing is expensive and time consuming and, as such, manufacturers and consultants are increasingly relying on simulation and modelling to reduce development times and the number of design iterations required.

One such consideration is the impact that changes made to exhaust system configurations and catalyst positioning, brought about by in-vehicle packaging constraints and design changes, can have on exhaust gas temperatures at the front face of the catalyst and, consequently, light-off times and drive cycle emissions. It would be beneficial if design engineers could predict the consequences of exhaust system changes on light-off times when assessing various alternatives.

To this end, a heat transfer model was constructed within the Matlab Simulink environment which could be used to predict exhaust gas temperatures based on exhaust port temperatures, flow rate and exhaust system geometry obtained experimentally or as an output from an engine simulation package such as GT-Power or Ricardo WAVE. The initial construction, underlying equations and assessment of this model is discussed in previous publications by the authors [[1], [2]]. A number of limitations of the original model were identified and discussed by the authors, and this study was undertaken to address these issues and thus, improve the operating range, accuracy and usability of the original model as well as introducing the ability to model twin skin exhaust sections with an air gap. A brief description of the model structure is given in this paper but, as already stated, further details can be found in previous publications [[1], [2]].

BRIEF MODEL OVERVIEW

Based on the methodology outlined by Konstantinidis *et al.* [4] and Buchner *et al.* [5] a model was developed to solve non-steady conduction within metal pipe sections.
Each modelled pipe section is split into 5 equal axial and radial elements with conduction equations solved for each based on the condition of the surrounding

sections. Using the example of an exhaust manifold flange, Figure 1 shows the energy flow into and out of the flange.

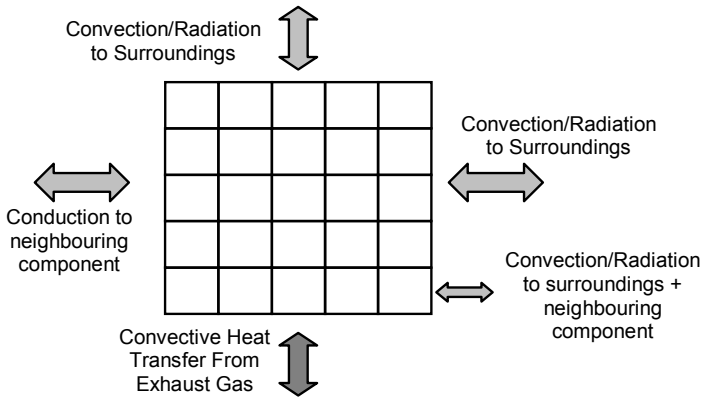

Figure 1 - Exhaust manifold flange energy flow pathways [2]

The 5 by 5 grid represents the quasi-finite element approach adopted to represent the conduction within the section under non-steady heat flow between the nodes. In addition, the energy flows associated with conduction to the head and adjacent pipe section, radiation and convection to the surroundings on the outer wall and convective heat transfer between the gas and inner wall of the section are included and solved via an energy balance including an energy storage term. Published relationships for free and forced convection to the surroundings [[4], [5], [6]] were included in the model. The degree of forced convection is dependant on the velocity of the air flowing over the pipe section as well as its wetted area.

ESTIMATION OF HEAT TRANSFER – A common way of describing the convective heat transfer relationship, between the exhaust gas and the inside of the pipe, is by examining the correlation between the Reynolds number (Re) of the gas and the Nusselt number (Nu). The Nusselt number is a dimensionless number used to measure the enhancement of heat transfer due to convection and can be expressed for a simple pipe section as:

$$Nu = \frac{h_{cv,i} D_i}{k_f}$$

Equation 1 – Nusselt Number Relationship

where $h_{cv,i}$ is the internal convective heat transfer coefficient, D_i is the internal diameter of the pipe section and k_f is the thermal conductivity of the fluid.

As the Nusselt number is a measure of the increased heat transfer due to convection, it follows that its value will be related to the state of the fluid flow to which the surface is exposed and thus, the Reynolds number. The general form of the Re/Nu relationship is given in Equation 2.

$$Nu = c_0 \, \mathrm{Re}^{c1} \, \mathrm{Pr}^{c2} \left(\frac{\mu_{bulk}}{\mu_{skin}} \right)^{c3}$$

Equation 2 - General form of Re/Nu Relationship

Where c_0, c_1, c_2 and c_3 are experimentally derived coefficients and μ denotes the fluid viscosity. Not all relationships described in other studies include the Prandtl number within the Reynolds-Nusselt relationship [7] and instead use the simplified relationship given in Equation 3

$$Nu = c_0 \, \mathrm{Re}^{c1}$$

Equation 3 - Simplified form of Re/Nu Relationship

Previous work by the authors [[1], [2]] describes the initial experimental determination of the coefficients in Equation 3 for various pipe section geometries and the construction of response surfaces which could be used to predict the coefficients based on pipe geometry.

Although not specifically addressed within the model, pulsations within the exhaust manifold runners are likely to lead to an increase in the convective heat transfer between the gas and the pipe wall, with a study by Dec and Keller finding that an increase in pulsation frequency and amplitude leads to an almost-linear increase in the Nusselt number, but that the effect diminishes with increasing Reynolds number [8]. While this effect may lead to small errors in predicted heat transfer within the exhaust manifold runners, experimental validation of the relationships showed good agreement with model predictions and should not, therefore, reduce the usefulness of the model.

SINGLE SKIN MODEL DEVELOPMENT

During a preliminary scoping project, relationships between the Nusselt and Reynolds numbers were derived for a series of straight and bend pipe sections of various wall thicknesses. This study is reported in a previous publication by the

authors [[1], [2]]. The accuracy of the initial model was limited due to the relatively few section geometries examined (four straight and seven bend sections), as well as the temperature and Reynolds number ranges being narrow to preserve the integrity of the instrumentation used. Figure 2 shows the measured Reynolds numbers within the exhaust manifold runner and downpipe of a VW group 1.8L turbocharged gasoline engine during the first 650 seconds of the US06 drive cycle, as well as the Reynolds number range examined and characterised for the test sections. It can be seen that the preliminary study only examined a very narrow range of Reynolds numbers, indicated by the horizontal lines between Re values of zero and approximately four thousand. While acceptable model accuracy was achieved under certain engine operating conditions, the model was unable to reliably predict the Re/Nu relationship, and hence heat transfer coefficient, outside of the modelled ranges. For this reason it was necessary to conduct a more thorough characterisation programme to address these shortcomings and improve the usability of the model.

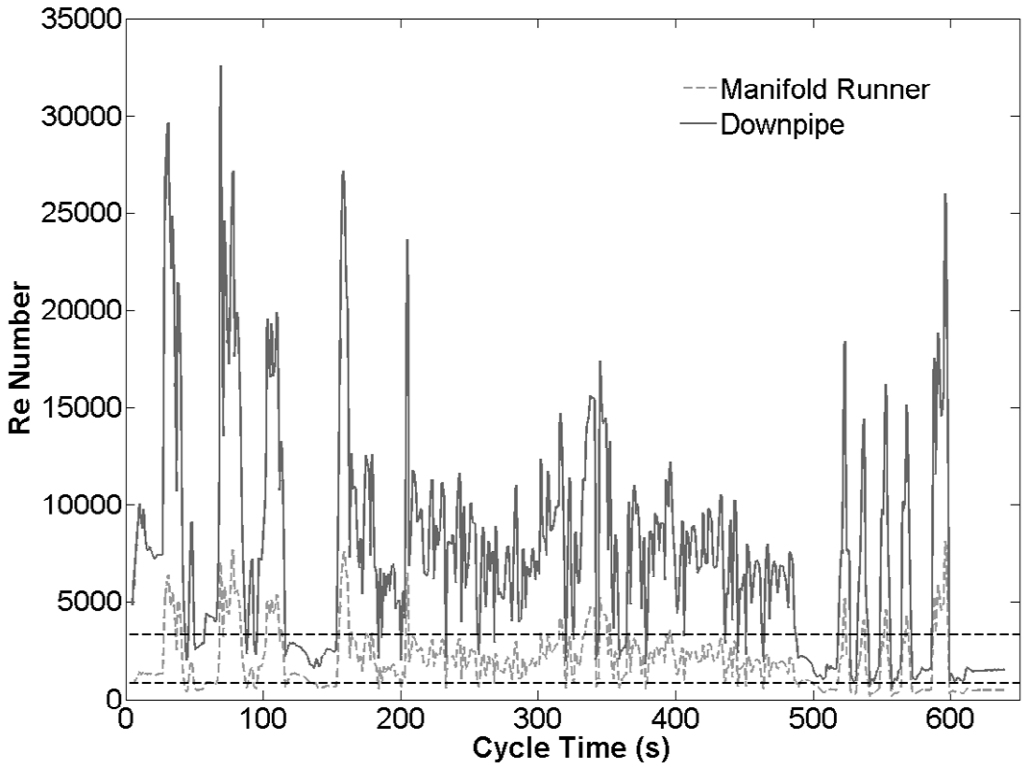

Figure 2 - Reynolds number range during US06 drive cycle

SINGLE SKIN SECTION CHARACTERISATION – Unlike during the preliminary experimental work, it was decided that experimental time could be reduced by testing multiple sections in series. Figure 3 shows a schematic representation of one of the bend sections with thermocouple locations. At each location, both the gas and wall temperatures were measured. It can be seen that within one experimental section there would be multiple geometries depending on which thermocouples were compared. For example, each test would simultaneously produce two repeats of a straight section (TC1-TC2 and TC6-TC7), four 45° bend sections (TC2-TC3, TC3-TC4, TC4-TC5 and TC5-TC6), two 90° bends (TC2-TC4 and TC4-TC6), one 135° section (TC2-TC5) and one 180° section (TC2-TC6).

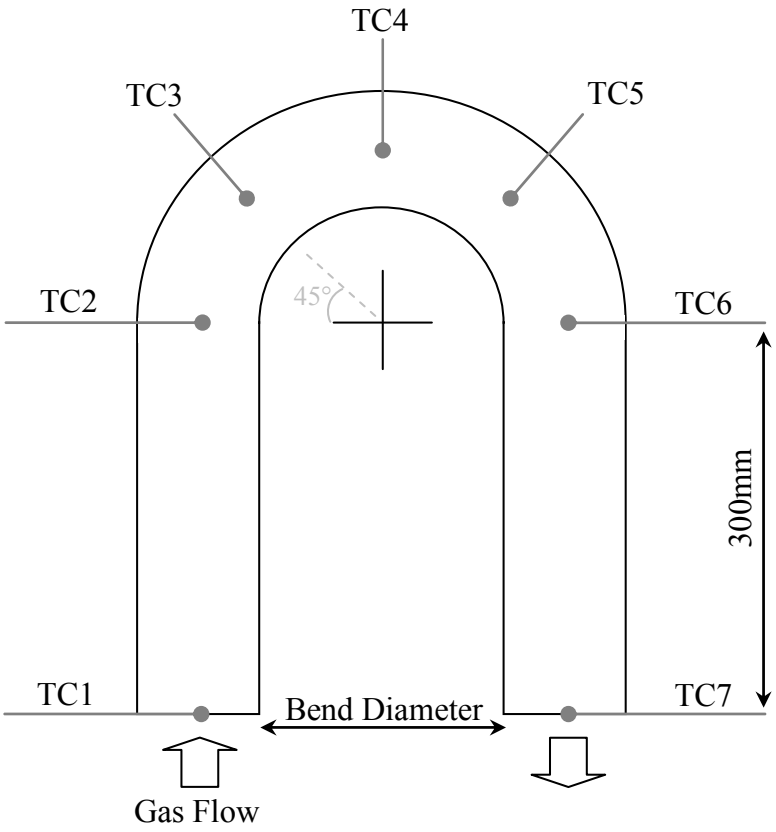

Figure 3 - Individual bend section layout

Fast response exposed junction thermocouples had previously been investigated and, while offering slight benefits in response, suffered from durability issues. For this reason 0.5mm stainless steel sheathed K-type thermocouples were used offering a good balance between response (due to low thermal inertia) and reliability.

In order to measure metal surface temperatures it was crucial to ensure a good contact between the thermocouple tip and the pipe surface. Preliminary work had suggested reliability issues with silver-soldering the thermocouples in position so an

alternative “patch” method was adopted. A very thin stainless steel patch was spot welded over the tip of the thermocouple in the desired location. Due to the low thickness, and small size, of the patch the small additional thermal inertia was not considered significant and was an acceptable trade-off with the improved robustness.

As with the preliminary study, the engine used for this work was a VW group 1.8 litre turbocharged gasoline engine directly coupled to a 200kW transient AC dynamometer. The engine however acted as little more than a hot gas generator during the section characterisation tests. Characterisation tests were carried out at a number of engine speed and load conditions, outlined in Table 1, designed to cover a wide range of exhaust gas Reynolds numbers. When comparing Table 1 and Figure 2 it can be seen that the bend section characterisation investigation will encompass all but the most extreme Reynolds numbers observed during the aggressive US06 drive cycle.

Table 1 - Steady state section characterisation engine test conditions (Reynolds numbers are approximate calculations at the outlet of the exhaust manifold)

Engine Speed RPM	Torque Nm	Reynolds Number #
800	0	1860
1000	20	2860
3000	20	5480
3000	40	7230
3000	60	8820
3000	80	10590
3000	100	12780
3500	120	17960
4000	150	25400

In order to validate the final model, each bend section was also tested over the initial 615 seconds of the US06 drive cycle shown in Figure 4. As all experimental work was conducted on a dynamic engine test facility, rather than in a vehicle, desired engine speeds and torques were matched with those previously measured when the same engine was tested in an Audi A4 vehicle on the University of Bath’s chassis dynamometer facility. Although a very good match was achieved, exact comparability between engine speeds and torques on the test bed and those seen in-vehicle was not essential as the validation phase was merely intended to assess the model predictions over a highly transient cycle.

After completion of the initial 615 seconds of the US06 cycle the engine was automatically set to a “daily check” condition of 2000 RPM, 2 bar BMEP and essential engine data recorded and compared with historical data to ensure consistency of engine operation over the extended duration of the experimental programme.

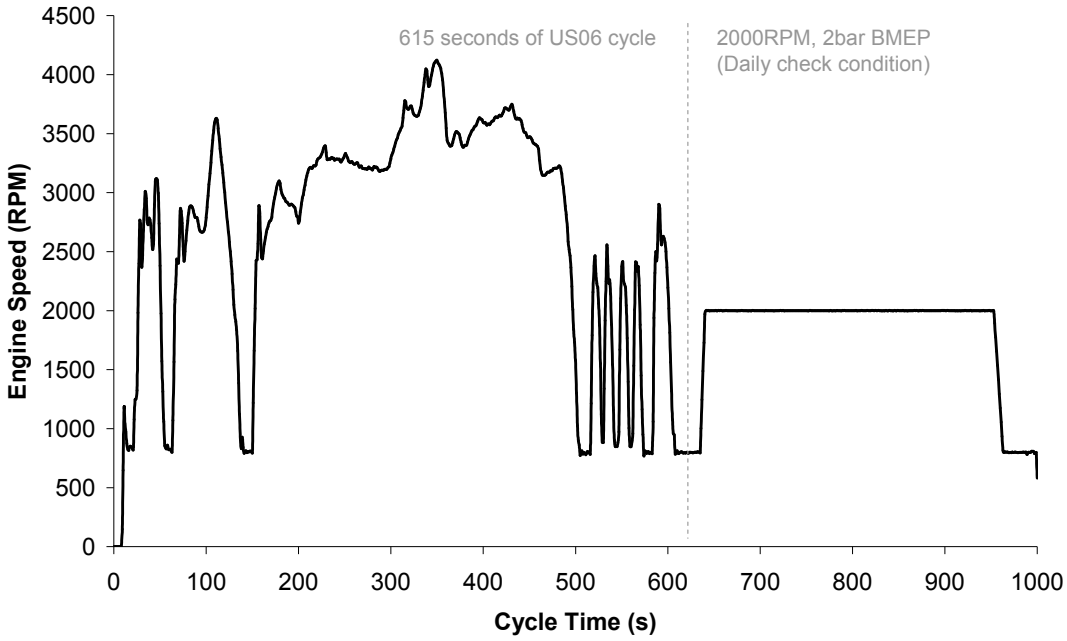

Figure 4 - Validation cycle

BEND SECTION RESPONSE MODELLING – An empirical model was constructed via the characterisation of numerous single-skin straight and bend exhaust sections relating the Nusselt number (and hence the heat transfer coefficient) to the section’s geometry and exhaust gas Reynolds number. The design inputs and responses are outlined in Figure 5 along with a graphical representation of the design space and test points. A list of the bend sections examined is given in Table 2.

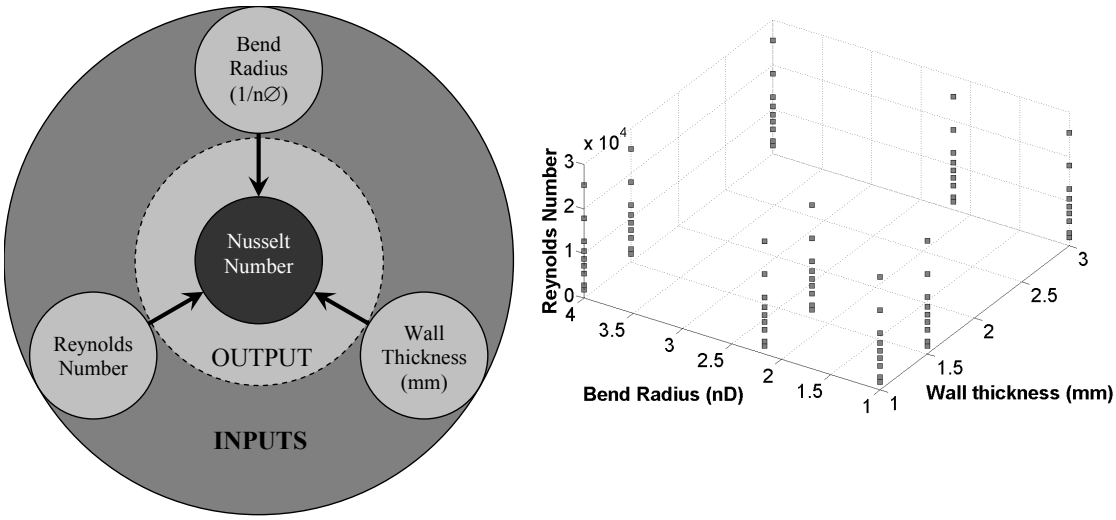

Figure 5 - DoE inputs, responses and design space (where nD is the number of pipe diameters)

Table 2 - Bend section geometries

Test Number	Wall thickness	Bend Radius	
(#)	(mm)	(mm)	(nØ)
1	1.5	38.10	1.00
2	1.5	82.55	2.17
3	3.0	38.10	1.00
4	1.0	82.55	2.17
5	1.0	152.40	4.00
6	1.5	152.40	4.00
7	3.0	152.40	4.00
8	3.0	82.55	2.17
9	1.0	38.10	1.00

Other changes made after consideration of the findings of the preliminary testing reported in the authors' previous publication [2] include:

- Pipe diameter was not included in the experimental design as this will be represented within the Reynolds number values.
- Bend radius was represented in terms of the number of pipe diameters (nD) rather than in metric units.
- In order to avoid issues with representing a straight section in terms of the bend radius, the model input was the reciprocal of the number of diameters, thus the value for a straight section would tend to zero rather than infinity.
- Bend angle was removed as an input as this is inferred by the bend radius and the section length and thus does not need to be included implicitly.

BEND SECTION REYNOLDS/NUSSELT RELATIONSHIPS – For each test section an iterative solver was included within the model in order to determine the Nusselt number required to achieve the measured temperature drop across the section for that Reynolds number.

By way of an example of the trends obtained, Figure 6 shows how the derived Reynolds-Nusselt relationship for sections, with a wall thickness of 1mm, varies with bend radius. It can be seen that, as expected, an increase in Reynolds number leads to an increase in the Nusselt number for all sections. Decreasing bend radius also leads to a marked increase in Nusselt number for a given Reynolds number reflecting the increase in convective heat transfer as the gas flow impinges on the pipe wall within the 'tighter' bends.

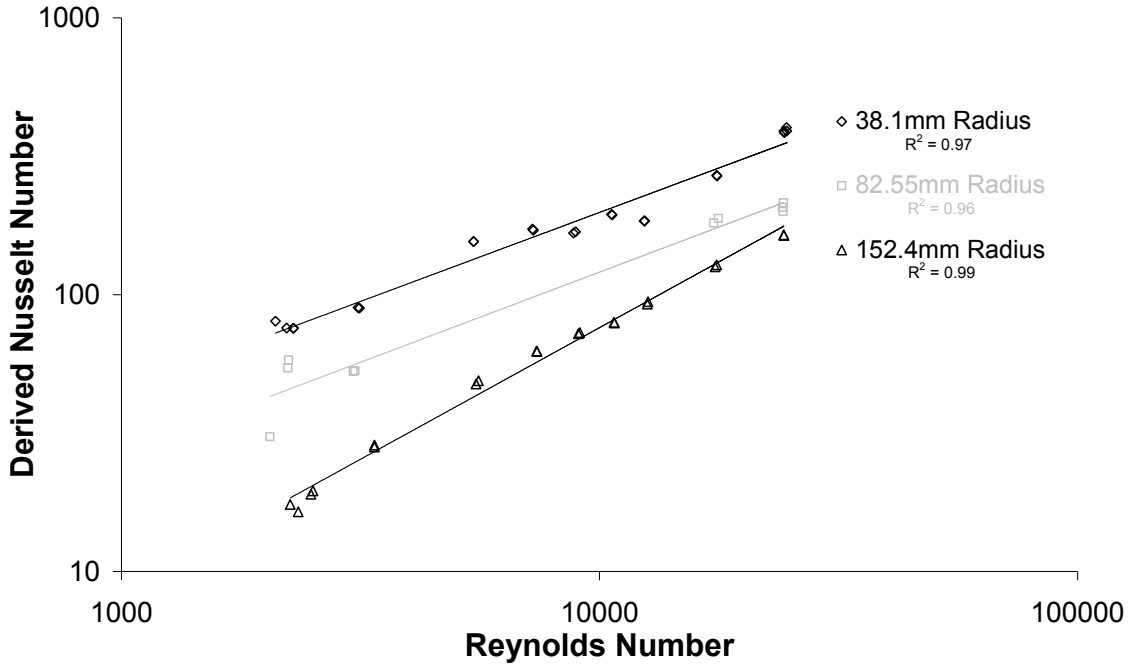

Figure 6 - Derived Nusselt relationships for 1mm wall thickness, 180° sections

Multi-variate analysis was performed on all collected data using the Matlab model based calibration toolbox. A second-order quadratic model was applied to the data with the response surfaces and model fit plot given in Figure 7.

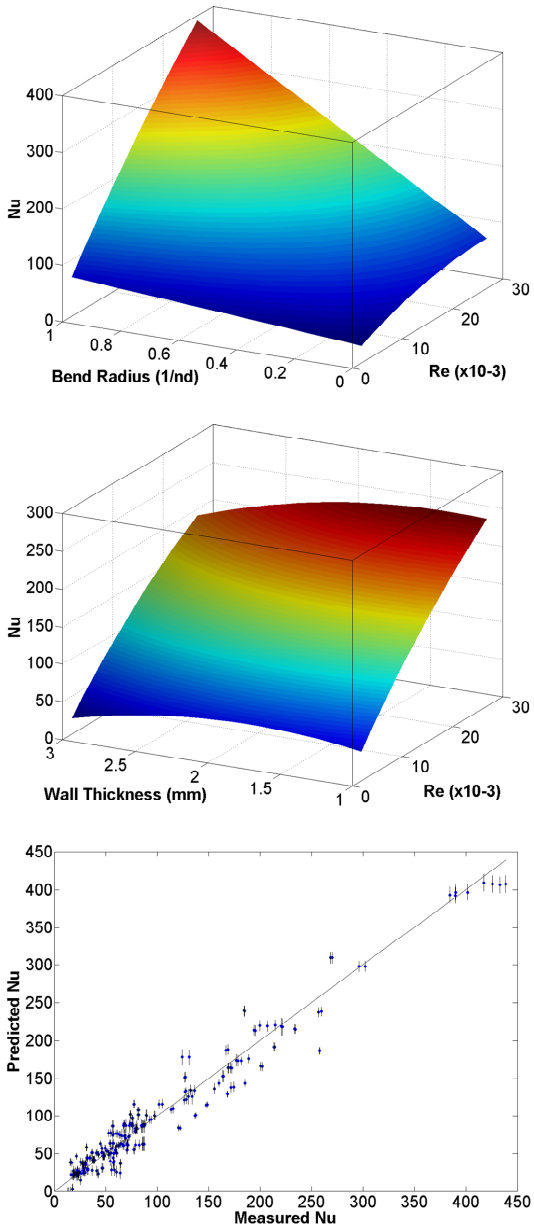

Figure 7 - Empirical exhaust gas to pipe wall response surfaces and model fit plot.

It can be seen in Figure 7 that the most dominant factor affecting Nusselt number is Reynolds number, however bend radius becomes increasingly significant with increasing Reynolds numbers. Wall thickness has minimal impact at low Reynolds numbers but does demonstrate a slight reduction in Nusselt number with increasing wall thickness at higher values of Re.

The response surfaces form the basis of the model allowing the prediction of the exhaust gas Reynolds-Nusselt relationship for previously unseen exhaust geometries within the experimental design region.

BEND SECTION MODEL VALIDATION – In order to assess the performance of the derived response models, and in turn the prediction of the heat transfer coefficient for different exhaust system geometries, the model was used to predict the exhaust system temperatures over the US06 drive cycle (as shown in Figure 4), with predictions compared to experimental data.

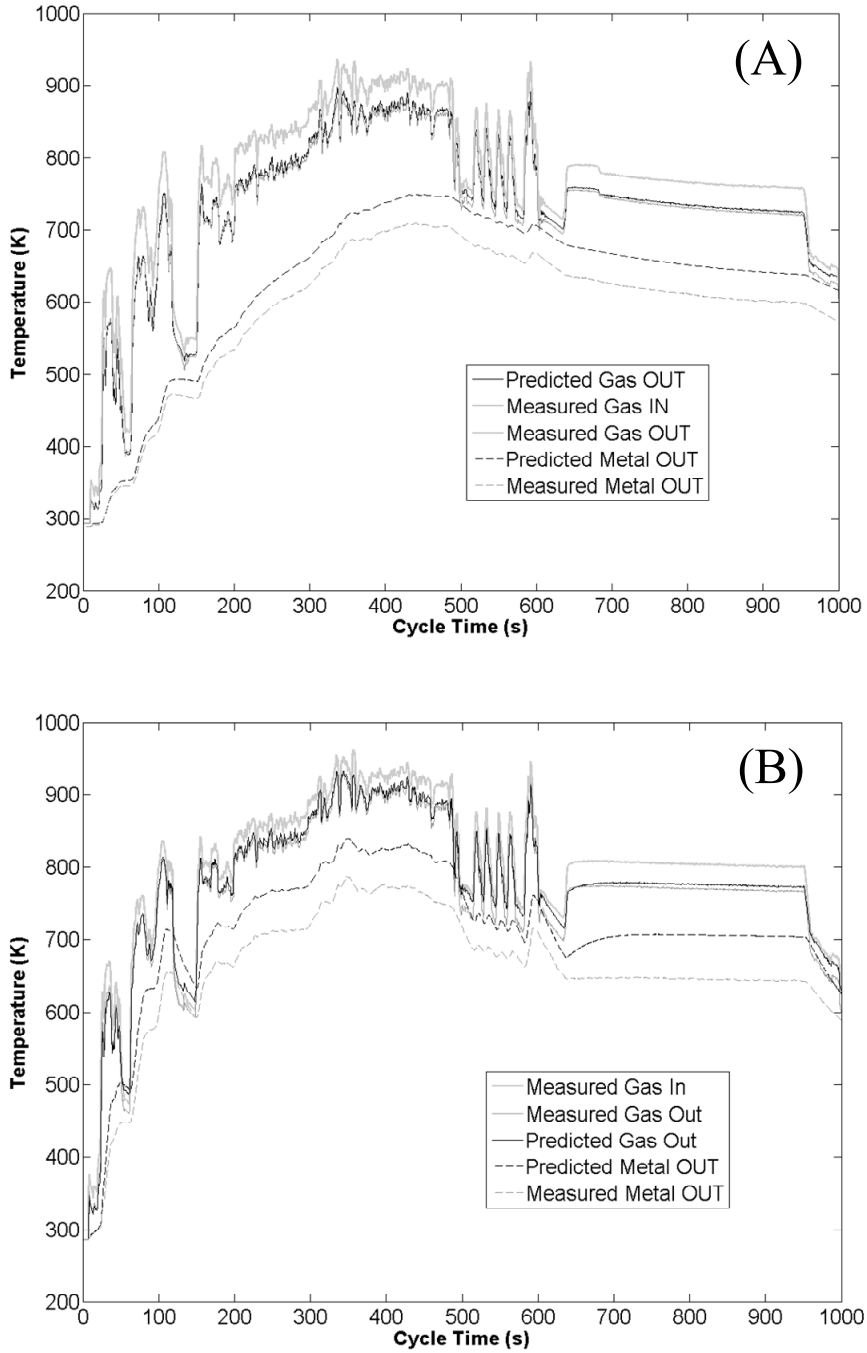

Figure 8 - Bend model validation: (A) Section 7: 3mm wall thickness, 152.4mm bend radius. (B) Section 4: 1mm wall thickness, 82.6mm bend radius.

Figure 8 shows the model predictions for two extremes of the design space, a 3mm wall thickness section with a bend radius of 152.4mm and a 1mm wall thickness section with a bend radius of 82.6mm. It can be seen that the predicted gas temperatures show very good agreement with measured data for the majority of the cycle, but with the largest errors apparent during idle periods when the Reynolds numbers drop to very low levels. Pipe wall temperature predictions, while following the same trends, do not match measured data to the same level of accuracy as the gas predictions, with the model consistently over-predicting the metal temperature. The discrepancies between predicted and actual metal temperatures will also contribute to the model under-predicting the temperature drop across the section during the idle periods mentioned previously due to the reduced temperature difference between the gas and the wall.

Figure 9 demonstrates the errors between predicted and measured data in a number of different ways to allow an assessment of the model performance to be made. Figure 9(A) shows the percentage error between actual and predicted gas and wall temperatures on a continuous basis during the validation US06 drive cycle (Figure 4). It can be seen that the error for predicted gas temperature is generally very low but with errors approaching 5% during idle periods. In a similar way Figure 9(B) shows the probability density for the gas errors during the validation cycle. As in Figure 9(A), it can be seen that, in general, the model slightly over-predicts the gas temperature with the mean error being approximately +1%, but with the idle period discrepancies causing the probability that the error falls between 3 and 5% to increase.

The probability density distribution is not quite the same as a histogram, instead, "*for a continuous random variable, the probability density function is represented by a curve such that the area under the curve between two numbers is the probability that the random variable will be between those two numbers*" [9].

Examining Figure 9(A) and Figure 9(C), it can be seen that the model over-predicts the section wall temperature for the majority of the cycle with errors typically falling between +8 and +16% and a mean error of approximately +10.5%. The probability density distribution shown in Figure 9(C) also displays a small amount of data between -1% and +2% error corresponding to the initial 20 seconds of the cycle when errors were low.

Finally, Figure 9(D) and Figure 9(E) show scatter plots of predicted versus actual gas and wall temperatures respectively during the validation cycle. For perfect model predictions the equation of the fit line through the data would be y=x, and it can be seen that the equation for the gas temperature fit (Figure 9(D)) shows a small

positive offset of +13°K, but a gradient very close to unity suggesting good model performance. The equation of the fit line in Figure 9(E) shows a positive gradient of 1.123 reflecting the fact that the model over-predicts the wall temperature as discussed earlier.

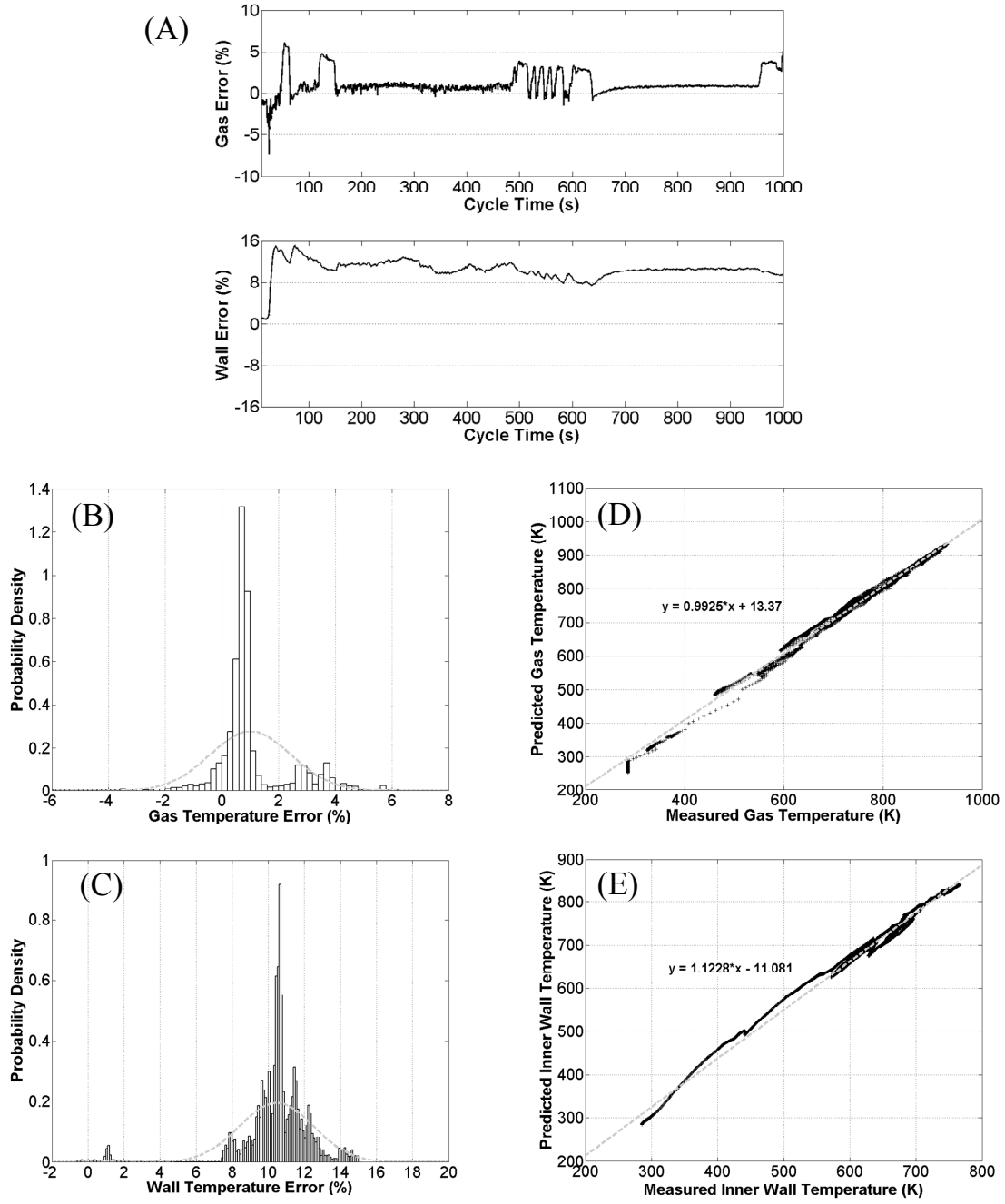

Figure 9 - Model error plots: Bend section 7 (3mm wall thickness, 152.4mm bend radius). (A) Instantaneous cycle Gas and Wall temperature error. (B) Probability density plot – Gas temperature error. (C) Probability density plot – Wall temperature error. (D) Predicted v Actual gas temperature. (E) Predicted v Actual wall temperature.

TWIN SKIN MODEL

The empirical model derived from the bend section characterisation study provided good predictions of exhaust gas temperatures for various exhaust configurations and geometries. In addition to single skin pipe sections, it would be of benefit if the model could be adapted to predict the heat transfer within twin skin systems.

Figure 10 shows a graphical representation of a twin skin section to be modelled along with the heat transfer modes present between the exhaust gas, skins, air gap and environment.

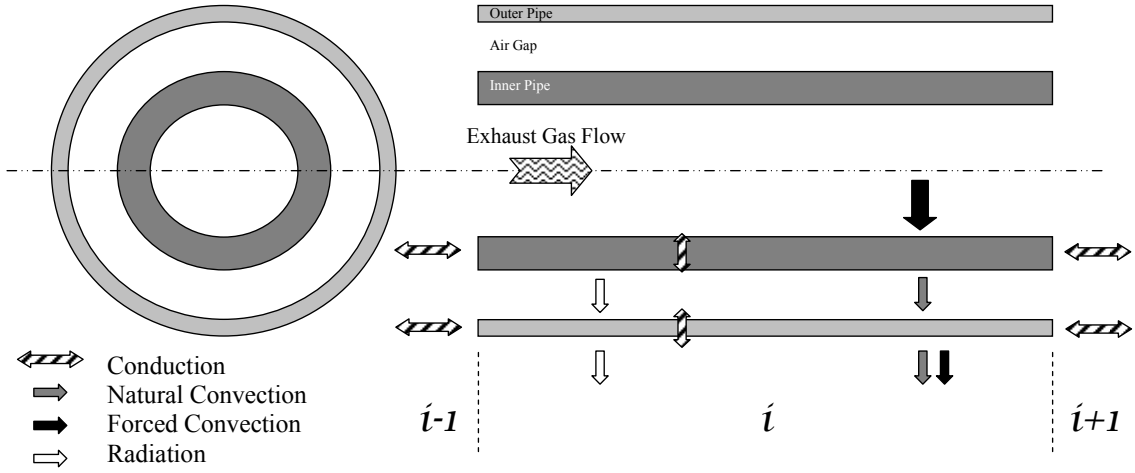

Figure 10 - Heat transfer modes in a twin skin exhaust section

As the ratio of section length to air gap is large the situation can be likened to two infinitely long concentric pipes, such that all radiated energy from one skin reaches the other. The limitation of this assumption would be in the case of bend sections where radiated energy could be emitted and absorbed by the same skin.

As with the single-skin model, each section skin is split into 5 axial and 5 radial elements thus improving wall temperature predictions for thicker-walled pipe sections.

EXPERIMENTAL CHARACTERISATION – 15 twin skin, stainless steel, exhaust sections were fabricated in order to characterise the impact that inner and outer skin wall thicknesses and air gap thickness had on heat transfer. Table 3 summarises the geometries of each section. The magnitude of wall thicknesses and the air gap were

chosen in order to be representative of the range of values which could potentially be observed within production vehicle exhaust systems.

Table 3 - Twin skin section geometries

Section Number #	Inner Skin Wall (mm)	Air Gap (mm)	Outer Skin Wall (mm)
1	0.8	4.0	0.8
2	2.0	4.0	0.8
3	0.8	8.0	0.8
4	2.0	8.0	0.8
5	0.8	4.0	3.0
6	2.0	4.0	3.0
7	0.8	8.0	3.0
8	2.0	8.0	3.0
9	0.8	6.0	2.0
10	2.0	6.0	2.0
11	1.5	4.0	2.0
12	1.5	8.0	2.0
13	1.5	6.0	0.8
14	1.5	6.0	3.0
15	1.5	6.0	2.0

Each section was assessed under the same steady state conditions as were used in the bend section characterisation study and detailed in Table 1. The engine used for the twin skin characterisation tests was a VW group 1.8 litre turbocharged gasoline engine directly coupled to a 200kW transient AC dynamometer.

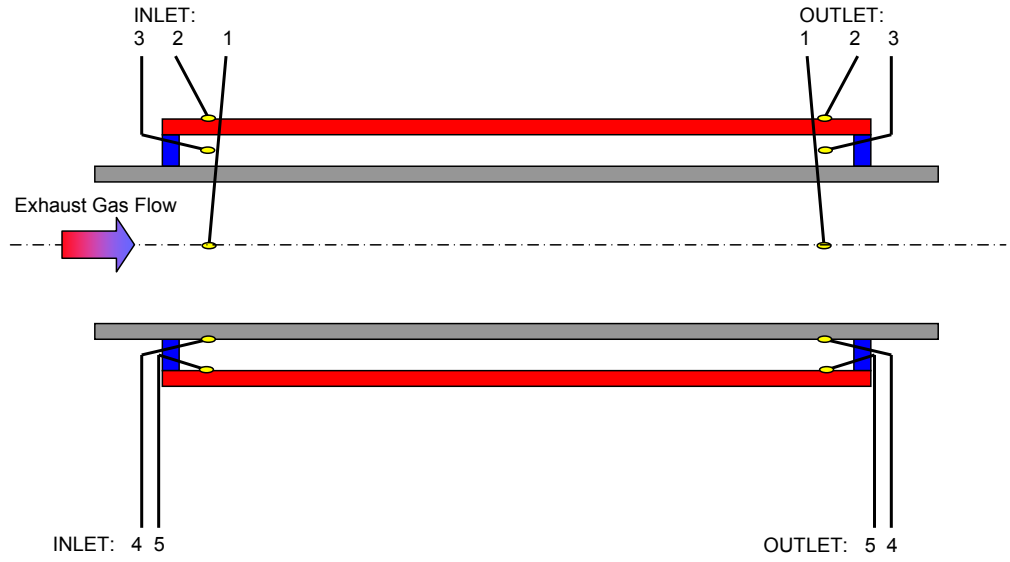

Figure 11 - Schematic of twin skin construction and thermocouple locations

Figure 11 shows a schematic of one of the twin skin sections with thermocouple locations at the inlet and outlet identified. In each case, the gas temperature, inner and outer wall temperatures and air gap temperature were measured.

Experimental data for use in validating the model performance was also gathered in the same way as with the bend section characterisation experiments using a portion of the US06 drive cycle (Figure 4).

TWIN SKIN MODEL DEVELOPMENT – Single skin model development work is discussed above and in a previous publication by the authors [2]. All previous versions of the model were developed for single-skin applications and needed to be adapted to cater for twin skin configurations.

Two validated single-skin models were combined to represent the inner and outer walls with new equations applied to represent the heat transfer between skins. In almost all automotive applications, while not specifically sealed, very little air flow will occur between the inner and outer walls, therefore heat transfer between them can be modelled as natural convection and radiation.

The radiated rate of heat transfer for a given section length can be expressed as:

$$\dot{q}_{rad,12} = \varepsilon\sigma\pi d_1\left(T_{p1}^4 - T_{p2}^4\right)\Delta i$$

Equation 4 – Rate of heat transfer via radiation

However, for two infinitely long concentric pipes the view factor, F, can be assumed to equal 1 so that the net radiation transfer from pipe 1 to pipe 2 equals the net rate of radiation transfer from pipe 1 as well as equalling the net rate of radiation transfer to pipe 2 [3]. This can be written as:

$$\dot{q}_{rad,12} = \dot{q}_{rad,1} = -\dot{q}_{rad,2}$$

Equation 5 - Net radiation heat transfer for concentric pipes

Therefore, in the case of a twin skin pipe section:

$$\dot{q}_{rad,12} = \frac{A_1\sigma\left(T_1^4 - T_2^4\right)}{\frac{r_1}{r_2}\left(\frac{1-\varepsilon_2}{\varepsilon_2}\right) + \frac{1}{\varepsilon_1}}$$

Equation 6 - Radiation heat transfer for twin skin pipe section [3]

An additional complication arises from the use of Equation 6, as the emissivity of a material can change with its temperature. Figure 12 shows how the emissivity of different materials changes with temperature. Of particular interest to this study is the impact that the oxidation state of stainless steel has on its emissivity. It can be seen in Figure 12 that the degree of oxidation not only affects the magnitude of the emissivity value, but also the characteristic "shape" of the response with respect to temperature. As specific emissivity data is not available for the stainless steel pipe sections used to fabricate the twin skin test sections, a relationship proposed by Konstantinidis *et al.* [4] was initially be applied within the model. This relationship is given in Equation 7 and is proposed to represent 304 grade stainless steel which has previously been heated to 500°C.

$$\varepsilon = \frac{0.54 + \left(T_P - 273\right)}{2830}$$

Equation 7 - Estimation of stainless steel emissivity [4]

Where T_p is the pipe temperature in degrees Kelvin.

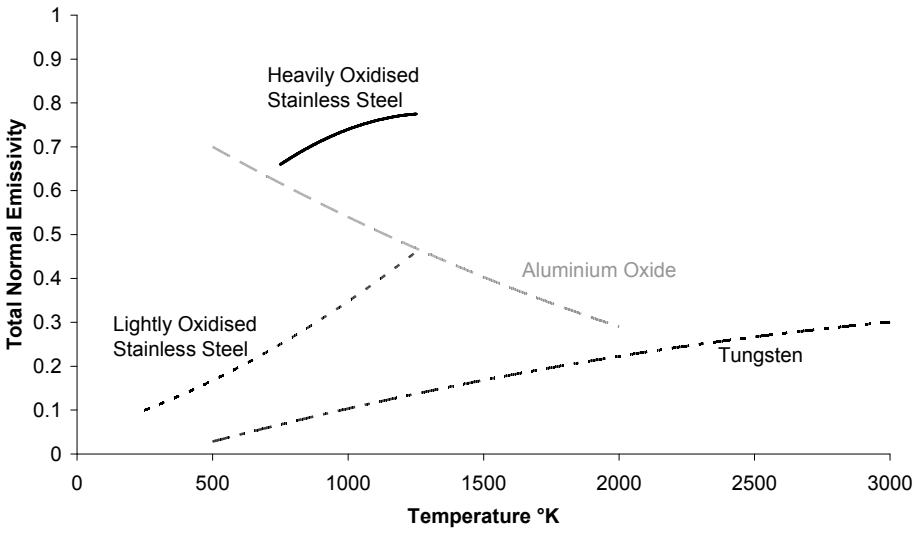

Figure 12 - The impact of temperature on emissivity for a number of materials (adapted from [3])

The other mode of heat transfer between the two skins of the section is natural convection. As with radiation, natural convection is calculated in relation to two infinitely long concentric pipes based on the method outlined by Konstantinidis *et al.* [4]. Details of the relationships used to calculate the heat transfer coefficient for natural convection across the air gap is given in APPENDIX 1.

INITIAL TWIN SKIN MODEL RESULTS – Figure 13 shows the model predictions for gas, inner wall and outer wall, compared with measured data. It can be seen that the model over-predicts the inner wall temperature leading to a reduced temperature gradient between the gas and wall and, as a result, slightly underestimates the heat loss from the gas as it passes through the test section. This implies that the model is not accurately representing the heat transfer between the inner and outer pipe skins.

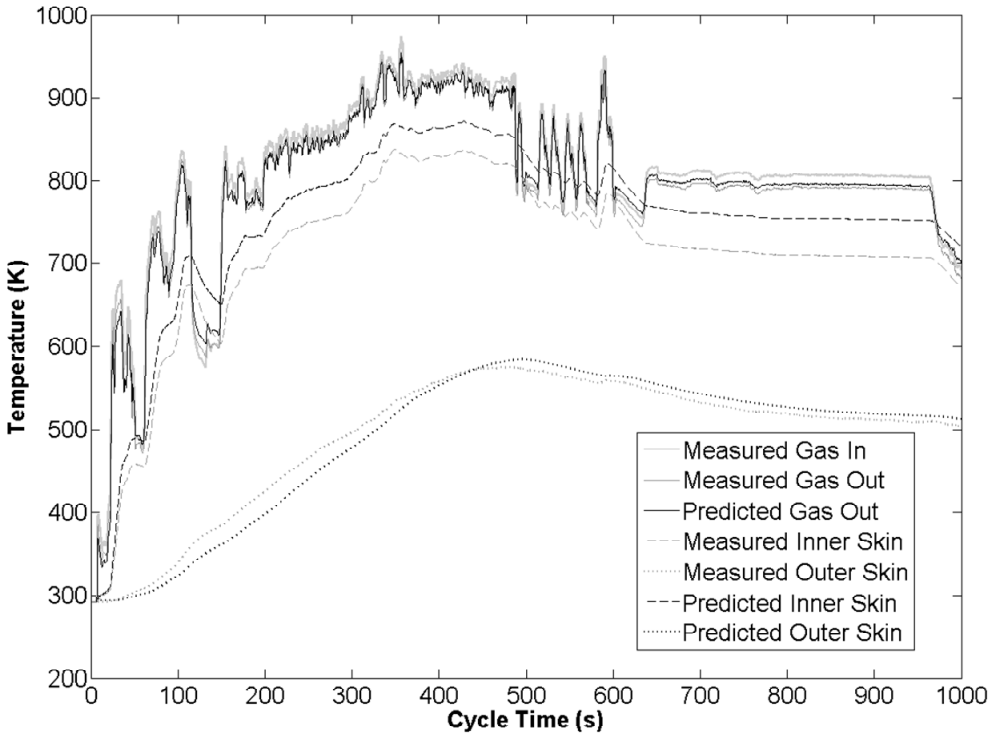

Figure 13 - Twin skin section 1 (inner=0.8mm, air gap=4mm, outer=0.8mm) predicted against measured temperatures

Figure 14 shows that, as the inner wall temperature increases, radiation far exceeds free convection as the dominant mode of heat transfer between the two skins and, as such, the over-prediction of inner wall temperature implies that the model estimation of emissivity is in error. In order to improve the model accuracy it was necessary to re-examine the emissivity relationship implemented within the model.

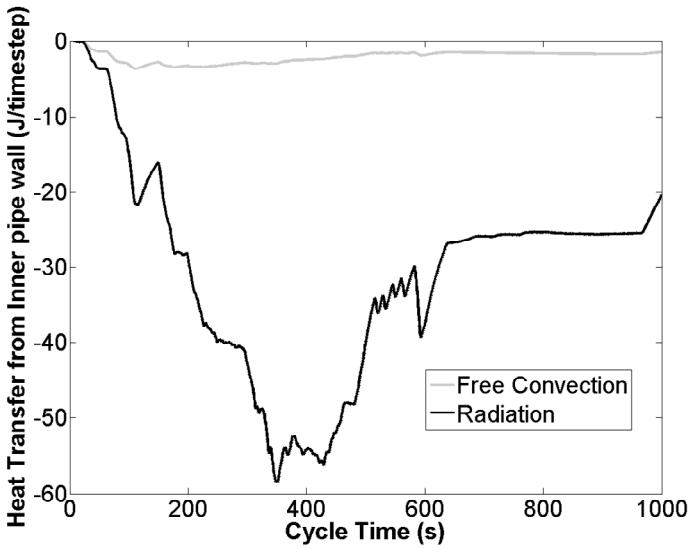

Figure 14 - Inner skin heat transfer for section 1 (inner=0.8mm, air gap=4mm, outer=0.8mm)

EMISSIVITY RELATIONSHIP – As was stated earlier, a simple relationship describing the change in stainless steel emissivity with increasing temperature had been used within the model to predict energy loss from the test section via radiation (Equation 7). During the bend section validation tests and those conducted on twin skin sections, the model consistently over-predicted the metal temperature (inner wall for the twin skin section) leading to a lower than predicted change in exhaust gas temperature. Errors in the emissivity estimate become increasingly significant for twin skin sections where radiation is the dominant form of heat transfer between metal skins.

Experimental steady-state data for single skin pipe sections was re-examined and the emissivity value tuned at each condition in order to minimise the pipe wall temperature errors. Figure 15 shows the experimentally-derived emissivity values for the polished 304L & 316L stainless steel straight sections as well as the original relationship used in the model (Equation 7).

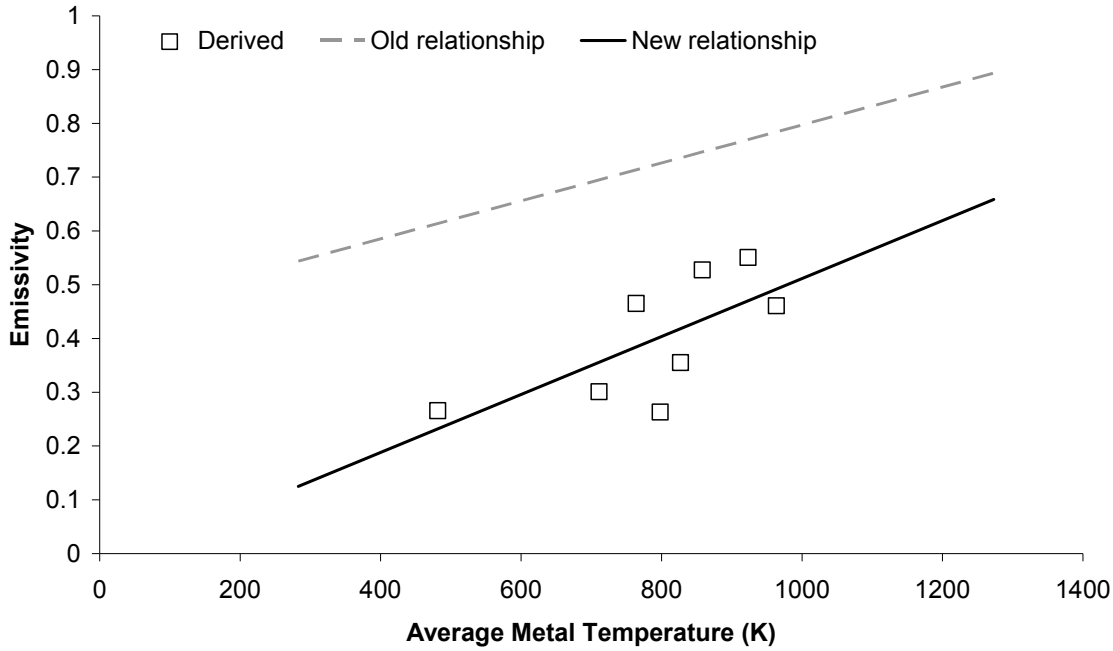

Figure 15 - Changes to pipe wall emissivity relationship (R^2=0.5)

Although the R^2 value is low for the fit line (R^2 = 0.5), it is clear that the derived emissivity values are significantly lower than those predicted using Equation 7, with the likely cause being the polished finish of the 304L and 316L stainless hygienic pipe used in this study. The revised emissivity relationship is given in Equation 8 and was adopted within the twin skin section model.

$$\varepsilon = 0.0005\, T_P - 0.0267$$

Equation 8 - Revised emissivity relationship for polished 304L stainless steel. Where T_P is the pipe temperature in °K

REVISED TWIN SKIN MODEL VALIDATION – After the derived emissivity relationship, given in Equation 8, was implemented within the model, revised twin skin section gas and wall temperature predictions could be made over the US06 validation cycle shown in Figure 4.

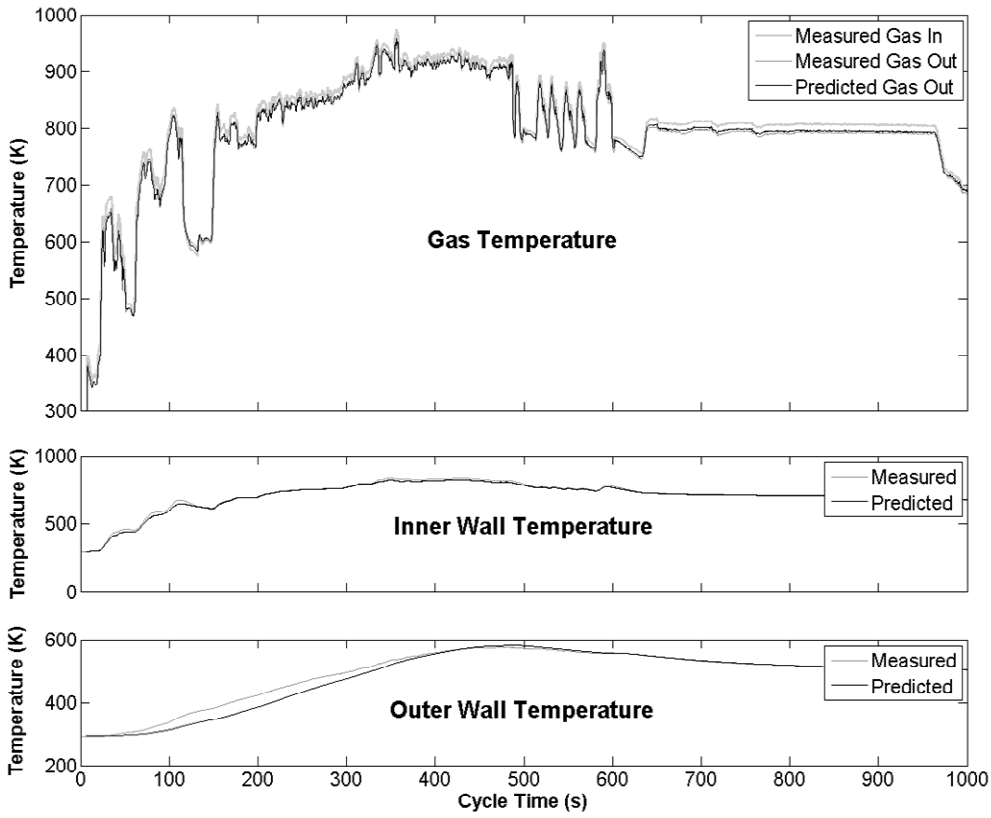

Figure 16 – Twin skin section 1 (inner=0.8mm, air gap=4mm, outer=0.8mm) predicted against measured temperatures with revised emissivity relationship.

Figure 16 shows the model predictions for gas, inner wall and outer wall, compared with measured data. This is the same section for which data was shown before the revised emissivity relationship was applied, and hence, a comparison of Figure 13 and Figure 16 demonstrate the impact this has made. Predicted exhaust gas temperature more closely follows the measured data, in particular during the idle periods of the cycle where the largest errors were observed with the original emissivity relationship. Inner and outer skin temperature predictions are markedly improved with inner skin temperature tracking measured data exceptionally accurately.

Model predictions for thicker walled sections demonstrate a slight reduction in the accuracy of wall temperatures, but gas temperature predictions still show good agreement with experimental data. Figure 17 shows an example of the model predictions of temperatures within a thicker-walled twin skin exhaust section.

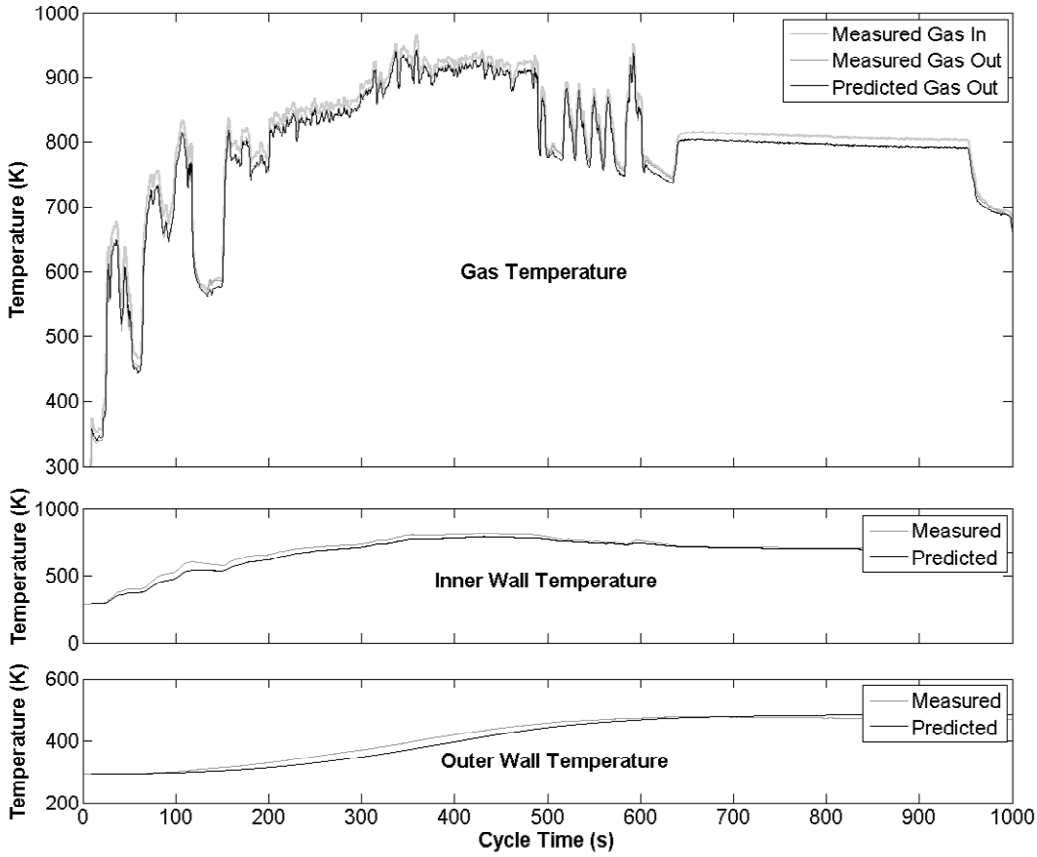

Figure 17 - Twin skin section 12 (inner=1.5mm, air gap=8mm, outer=2.0mm) predicted against measured temperatures with revised emissivity relationship.

As in Figure 9, Figure 18 demonstrates the errors between predicted and measured data in various ways to allow an assessment of the model performance to be made. Figure 18(A) shows the percentage error between actual and predicted gas and wall temperatures on a continuous basis during the validation US06 drive cycle (Figure 4). Comparing Figure 18 with Figure 9, it is clear that the revised emissivity relationship has improved the accuracy of the model significantly, in particular gas temperature errors during idle periods. Figure 18(B) and Figure 18(E) show that the range of gas temperature errors has been reduced to approximately ±1% with a mean error of +0.2% while predicted against actual temperatures demonstrate a near-perfect y=x relationship. Inner wall temperature predictions show a mean error of -1% (Figure 18(C)) but, as can be seen in Figure 18(A), the model under-predicts the inner wall temperature during the initial 100 seconds of the cycle, after which time, predictions fall within ±2%. Figure 18(F) shows predicted versus actual inner wall temperatures and displays good agreement but with a slight negative offset of -8.3°K.

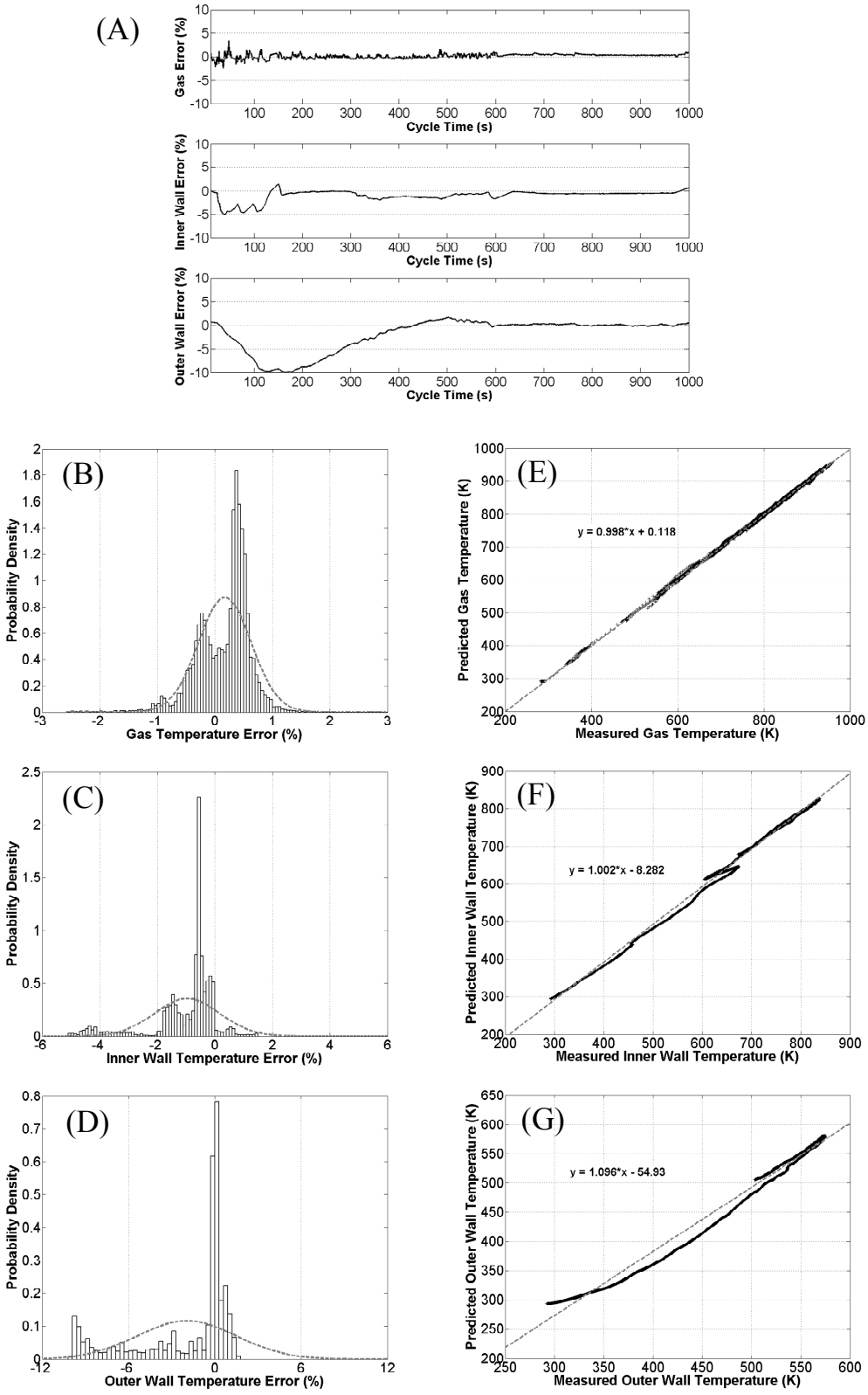

Figure 18 - Model error plots: Twin skin section 1 (inner=0.8mm, air gap=4mm, outer=0.8mm). (A) Instantaneous cycle Gas, inner and outer wall temperature error. (B) Probability density plot – Gas temperature error. (C) Probability density plot – Inner wall temperature error. (D) Probability density plot – Outer wall temperature error. (E) Predicted v Actual gas temperature. (F) Predicted v Actual inner wall temperature. (G) Predicted v Actual outer wall temperature.

Unlike Figure 9, which only presented data for a single skin bend section, Figure 18 also shows the model errors relating to the twin skin section's outer wall temperature predictions (Figure 18: A, D & G). As with the inner wall temperature predictions, the model slightly under-predicts the outer wall temperature during the early part of the cycle reaching a maximum error of -10% before the error gradually reduces as the predicted and actual temperatures converge (also shown in Figure 16). Outer wall predictions show a mean error of approximately -2.5%, but with errors of less than ±2% for the majority of the cycle.

CONCLUSIONS

The heat transfer model constructed to predict the impact that exhaust system geometry would have on exhaust gas heat transfer and, ultimately, catalyst light-off described in a previous publication by the authors [2] has been further developed to improve the accuracy of predicted data and allow the modelling of twin skin exhaust sections. The following conclusions can be gleaned from this study:

- Additional experimental characterisation of single-skin bend sections over extended Reynolds number and temperature ranges has improved the usefulness and accuracy of model predictions compared with previously published data [[1], [2]].
- Exhaust gas temperature predictions for single-skin bend sections showed errors of less than ±5% over the initial portion of the US06 drive cycle.
- The model over-predicted single-skin wall temperatures by approximately 10% over the US06 cycle before modifications to the emissivity relationship of the metal used in this study.
- The model was developed to include twin skin exhaust sections and the natural convection and radiation between skins. As with the single-skin sections, the model initially over-estimated the wall temperatures leading to a lower than expected temperature difference between the gas and the wall and a slight over-prediction of gas temperature.
- Radiation was identified as the dominant form of heat transfer between the inner and outer walls of twin skin sections, and thus, the most likely cause of an over-prediction of inner wall temperature.
- A revised relationship governing the change in the emissivity of the section wall with temperature was derived from experimental data and applied within the model.

- The final model demonstrated improved accuracy of exhaust gas predictions with typical errors of less than ±1% and a mean error over the US06 cycle of +0.2%. The model slightly under-predicts inner wall temperature of twin skin sections with typical errors falling between zero and -2%. Outer wall temperature predictions show good agreement with experimental data (approximately ±2% error) for the majority of the US06 cycle but an under-prediction during the initial 300 seconds with a maximum error of less than 10%.

Further publications by the authors will address the practical impact of twin skin wall thicknesses and air gap size on exhaust gas temperatures drop as well as additional work conducted to investigate the impact of gasoline catalyst heating strategies, leading to exotherms within the exhaust system, on light-off times and predicted exhaust temperatures.

REFERENCES

[1] Bannister, C.D., Brace, C.J., Taylor, J., Brooks, T. and Fraser, N., Experimental Characterisation of Heat Transfer in Exhaust Pipe Sections; SAE Paper 2008-01-0391, 2008.

[2] Bannister, C., Brace, C., Taylor, J., Brooks, T., Fraser, N., 2009. The use of multi-variate models for the prediction of heat transfer in vehicle exhaust systems. Proceedings of the Institution of Mechanical Engineers, Part D: Journal of Automobile Engineering, 224 (3), pp. 369-385.

[3] Cengel, Y. A., 1997. Introduction to thermodynamics and heat transfer. London: The McGraw-Hill Companies Inc.

[4] Konstantinidis, P. A., Kolsakis, G. C. and Stamatelos, A. M. Transient heat transfer modelling in automotive exhaust systems; Proc. Instn Mech. Engrs., Part C, Journal of Mechanical Engineering Science, 1997 211 (C1), 1-15.

[5] Buchner, S., Santos Lardies, S., Degen, A., Donnerstag, A. and Held, W. A modular numerical simulation tool predicting catalytic converter light-off by improved modelling of thermal management and conversion characteristics; SAE Paper 2001-01-0940, 2001.

[6] Eriksson, L. Mean value models for exhaust system temperatures; SAE Paper 2002-01-0374, 2002.

[7] Shayler, P.J., Hayden, D.J. 1999. Exhaust system heat transfer and catalytic converter performance; SAE International, Paper No. 1999-01-0453.

[8] Dec, J.E., Keller, J.O., 1989. Pulse combustor tail pipe heat transfer dependence on frequency, amplitude, and mean flow rate. Combust. Flame, 77 pp. 359–374.

[9] Definition of the Probability Density Function [online]. Available from: (http://www.answers.com/topic/probability-density-function) [Accessed 17/8/2010].

AKNOWLEDGMENTS

This work has been conducted at the Powertrain and Vehicle Research Centre in the Department of Mechanical Engineering at the University of Bath in conjunction with Mahle Powertrain UK.

CONTACT

Dr Chris Bannister
Department of Mechanical Engineering
University of Bath
Bath BA2 7AY
UK.
E-mail: C.D.Bannister@bath.ac.uk
Web: www.pvrc.co.uk

NOTATION

α	Thermal diffusivity (m^2s^{-1})
β	Thermal expansion coefficient
ε	Emissivity
λ	Thermal conductivity (W/m.K)
ν	kinematic viscosity (m^2s^{-1})
σ	Stefan-Boltzmann constant ($W.m^{-2}.K^{-4}$)
A	Surface area (m^2)
d	Diameter (m)
F	View factor

g	Gravitational acceleration (ms^{-2})
h	Heat transfer coefficient ($W/m^2.K$)
i	Unit length
Nu	Nusselt number
q	Heat transfer rate (J/s)
r	Radius (m)
Ra	Rayleigh number
Re	Reynolds number
s	Air gap thickness (m)
T	Temperature (°K)
T_P	Pipe temperature (°K)

APPENDIX 1

The following relationships are used to represent natural convection between two infinitely long concentric pipes and are valid for values of Ra > $7.1x10^3$. [4]

$$h_{gap} = \frac{Nu_{gap}\lambda_{gap}}{s_{gap}}$$

Where:

$$s_{gap} = \sqrt{(r_1 r_2)}\ln\left(\frac{r_2}{r_1}\right)$$

and:

$$Nu_{gap} = 0.2Ra^{0.25}\left(\frac{d_2}{d_1}\right)^{0.5}$$

where:

$$Ra_{gap} = \frac{s_{gap}^3 g\beta_{gap}\left(T_{p1} - T_{p2}\right)}{\alpha_{gap}\nu_{gap}}$$